JOURNAL OF MATERIALS SCIENCE: MATERIALS IN MEDICINE 15 (2004) 261–265

Effects of alkali pretreatment of silk fibroin on microstructure and properties of hydroxyapatite–silk fibroin nanocomposite

LI WANG, REI NEMOTO, MAMORU SENNA*
Department of Applied Chemistry, Faculty of Science and Technology, Keio University, 3-14-1 Hiyoshi, Yokohama 223-8522, Japan
E-mail: senna@applc.keio.ac.jp

Nanocomposites comprising hydroxyapatite (HAp) and silk fibroin (SF) were synthesized from $Ca(OH)_2$ suspension co-dispersed with SF fine particles and H_3PO_4 solution via a wet-mechanochemical route. The SF particles were modified with an alkali solution to increase contact points between HAp phase and SF matrix. HAp crystallites grow more preferentially along *c*-axis on alkali pretreated SF substrates. The composites exhibit porous microstructure with 70% of open porosity and about 70% of the interpores ranging from 40 to 115 μm in diameter. The peak shifts in amide II band of SF indicate that the chemical interactions between HAp crystals and SF matrix are intensified by the alkali pretreatment of SF. The stronger inorganic-organic interactions promote the formation of three-dimensional network extending throughout the composites, bringing about an increase of 63% in the Vickers hardness to the composite.

1. Introduction

Hydroxyapatite (HAp) has been widely used in bone tissue engineering and dental prostheses since it is the principal mineral component of natural bones and teeth with excellent biocompatibility, osteoconductivity and bioactivity. It is well documented that natural bones comprise approximately 70 wt % HAp and 30 wt % organics, in which HAp nanoparticles are uniformly arranged within the organic matrix in a complex hierarchical manner [1–3]. It is this unusual intimate synergy between inorganic phase and organic matrix that endows native bones with sufficient mechanical toughness and flexibility to serve as scaffolds of human body. However, a single phase HAp cannot meet the functional needs of bone implants due to its brittleness and associated low mechanical toughness. Attempts have been therefore made to develop alternative composite biomaterials by bending HAp particles with some mechanical strong polymers over several decades.

Bonfield *et al*. has been engaged in the development of HAp-reinforced polyethylene composite since early 1980s [4] and achieved two successful biomedical applications of this material in orbital floor prostheses and middle-ear implantation [5, 6]. Polyethylene has attractive mechanical properties, but is biologically inert. It is of great challenge to devise and fabricate a new generation of HAp-based composite biomaterials having comparable microstructure and properties with natural bone along with high bioaffinity to improve the interaction and attachment between implants and host surrounding tissues. Recently, increasing efforts have been therefore focused on the involvement of some biopolymers or proteins with favorable biocompatibility, bioactivity and bioaffinity, such as collagen [1–3, 7], silk fibroin [8, 9], gelatin [10], chitosan [11, 12] or chondroitin sulfate [13, 14], in HAp-based composites.

Silk fibroin (SF), a hard protein extracted from silk cocoon, is composed of 17 amino acids. SF with β-sheet structure has been applied in wound dressing area due to its sufficient mechanical strength, appreciable bioaffinity, and good oxygen permeability [15–17]. Compounding HAp with SF is, therefore, expected to show enhanced bioaffinity and mechanical toughness as well as improved osteoconductivity.

In our previous study [9], we found that HAp nanocrystals are self-assembled along *c*-axis and a three-dimensional network is formed throughout the composite via the crosslinkage between HAp crystallites and SF substrates. The purpose of the present study is to increase the interfacial contact number density, and hence to improve the crosslinkage between mineral phase and organic matrix. We therefore chemically modified SF surface with an alkali solution prior to the preparation of HAp–SF nanocomposite sol. Furthermore, we investigated the effects of the alkali pretreatment of SF on crystallographic properties of HAp, chemical states, microstructure, and microhardness of the composite.

*Author to whom all correspondence should be addressed.

2. Experimental procedure

Ten grams of SF powders (Lot: 98, donated by Idemitsu Petrochemical Inc.) with β-sheet structure and average particle size of 7.9 μm were immersed into 200 ml NaOH solution of 0.05 M and stirred at room temperature for 2 h. After incubation in a water bath at 45 °C for 24 h, the suspension was centrifuged and washed by deionized water alternately for several cycles until the discarded supernatant was neutral. Then we obtained the alkali pretreated SF (denoted as ASF).

$Ca(OH)_2$ (Wako Pure Chemical Inc.), H_3PO_4 (Taisei Pure Chemical Inc.) of analytic grade, and untreated SF (denoted as USF) or ASF were employed as starting materials. Fifty-milliliter H_3PO_4 solution of 4.4 M was added dropwise into 178 g of 16 wt % $Ca(OH)_2$ suspension co-dispersed with 3.7 g SF (10 wt % of HAp). The molar ratio of Ca/P in the starting mixture was set as 1.67, equal to that of the stoichiometric HAp. The mixture was stirred vigorously for 1 h and then milled at room temperature by a multi-ring mill (MICROS-0, Naro Machinery) at 1250 rpm for 3 h. The detailed grinding mechanism of the milling apparatus was described elsewhere [18]. The as-milled composite sol was washed by distilled water and centrifuged alternately for 3 cycles, followed by vacuum drying at 50 °C for 24 h. The two samples attained from USF and ASF were symbolized as HA-USF and HA-ASF, respectively.

The as-prepared powders were examined by X-ray diffractometer (XRD) (RINT 2200, Rigaku Co., Tokyo) with CuKα radiation. The X-ray diffraction data were collected in 2θ range of 10–120° with a step size of 0.05° and a counting time of 10 s. These data were refined by Rietveld analysis using a computer program RIETAN 2000 developed by Izumi and Rigaku Co. Ltd. [19] to determine crystallographic parameters of HAp. Functional groups in the composites were probed by Fourier transformed infrared (FTIR) spectroscopy (BIO-RAD, FTS-60A/896). A scanning electron microscope (SEM, Hitachi, S-4700) was used to observe microstructure. Pore size distribution was evaluated by mercury porosimetry (CE Instrument, PASCAL140 and PASCAL440).

Microhardness of the samples was measured by means of a Vickers hardness tester (AKASHIMVK-F II). Powder samples were compressed into cylindrical tablets with a diameter of 11.3 mm and a height of 3.6 mm under a uniaxial pressure of 196 MPa for 3 min. A pyramidal diamond indenter was applied to the surface of the tablet under a 50 g load for 15 s. Diagonal length of the indentation was measured through a micometric eyepiece with an objective lens of 40X. The tests were repeated 10 times for each sample. The Vickers hardness number was calculated using the equation $VHN = (2F \sin\theta/2)/d^2$, where F is the applied load in grams, θ is the angle between opposite faces of indenter (136°), and d is the diagonal length of indentation in micrometers.

3. Results and discussion

From the XRD patterns shown in Fig. 1, the inorganic component of the composites is identified as monophase crystalline HAp. Table I clearly indicates that the two

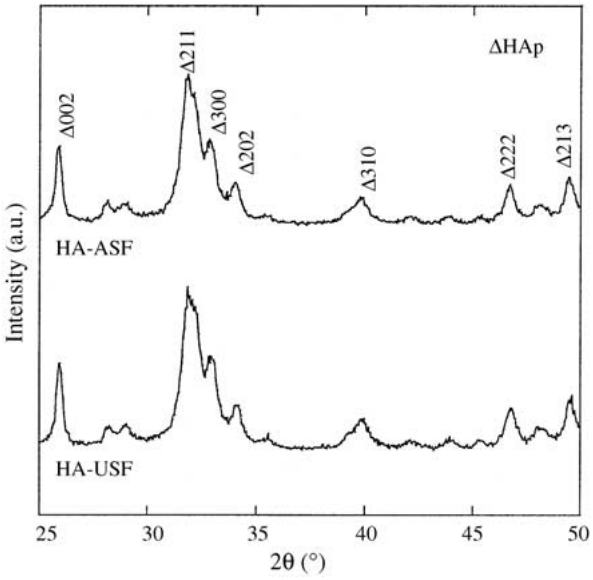

Figure 1 XRD profiles of HA-USF and HA-ASF composites.

samples are very similar in their crystallographic parameters along a-axis, L_a, ε_a, and lattice constants. Along c-axis, however, their crystallographic parameters significantly differ from each other. From HA-USF to HA-ASF, the aspect ratio, L_c/L_a, and the lattice microstrain, ε_c, increase by 22% and 72%, respectively. This demonstrates that the HAp crystallites in HA-ASF composite show more anisotropic growth with higher extent of lattice imperfection along c-axis. Thus, the preferential orientation of HAp crystallites along c-axis is promoted by the alkali pretreatment of SF. The greater lattice imperfection is interpreted, if partly, as the incorporation of residual sodium ions in the alkali pretreated SF into HAp structure by replacing calcium ions [20].

The effects of the alkali pretreatment of SF on chemical states of the composites are evaluated by FTIR spectra as shown in Fig. 2. The absorption bands at 1628 cm^{-1} (amide I), 1520 cm^{-1} (amide II) and 1233 cm^{-1} (amide III) in Fig. 2(a) are characteristic of the β-sheet structure of SF [13]. There is no obvious peak shift found from USF to ASF, indicating that the chemical states of SF are not altered the alkali pretreatment. In Fig. 2(b), we observe a broad peak at 1639 cm^{-1} in HA-USF and 1643 cm^{-1} in HA-ASF, respectively. This broad peak is presumably attributed to the overlap of OH group at 1640 cm^{-1} in HAp and amide I band in SF. From SF to the composite, amide III band remains unchanged. However, amide II band shifts to higher wave numbers (Fig. 2(c), i.e. the blue shifts by ca. 7 cm^{-1} from SF to HA-USF, ca. 13 cm^{-1} from SF to HA-ASF, respectively. It is evident that the blue shift in amide II band becomes larger with the alkali pretreatment of SF. These findings suggest that the strong chemical interactions exist between HAp and SF, most probably between calcium ions of HAp and amide groups of SF [2, 7, 14], and are intensified by the alkali pretreatment of SF.

From the SEM micrographs displayed in Fig. 3, we observe HAp crystallites aggregate into clusters and are connected with SF fibrils to form three-dimensional porous microstructure in the composites. With ASF

TABLE I Crystallographic parameters of HAp crystals

Sample	L_c* (nm)	ε_c** (%)	L_a* (nm)	ε_a** (%)	L_c/L_a	a (Å)	c (Å)
HA-USF	18.8	0.25	9.81	0.50	1.91	9.428	6.889
HA-ASF	22.0	0.35	9.51	0.50	2.31	9.432	6.890

*L_c or L_a represents the crystalline size along c-axis or along a-axis.
**ε_c or ε_a represents the lattice microstrain along c-axis or along a-axis.

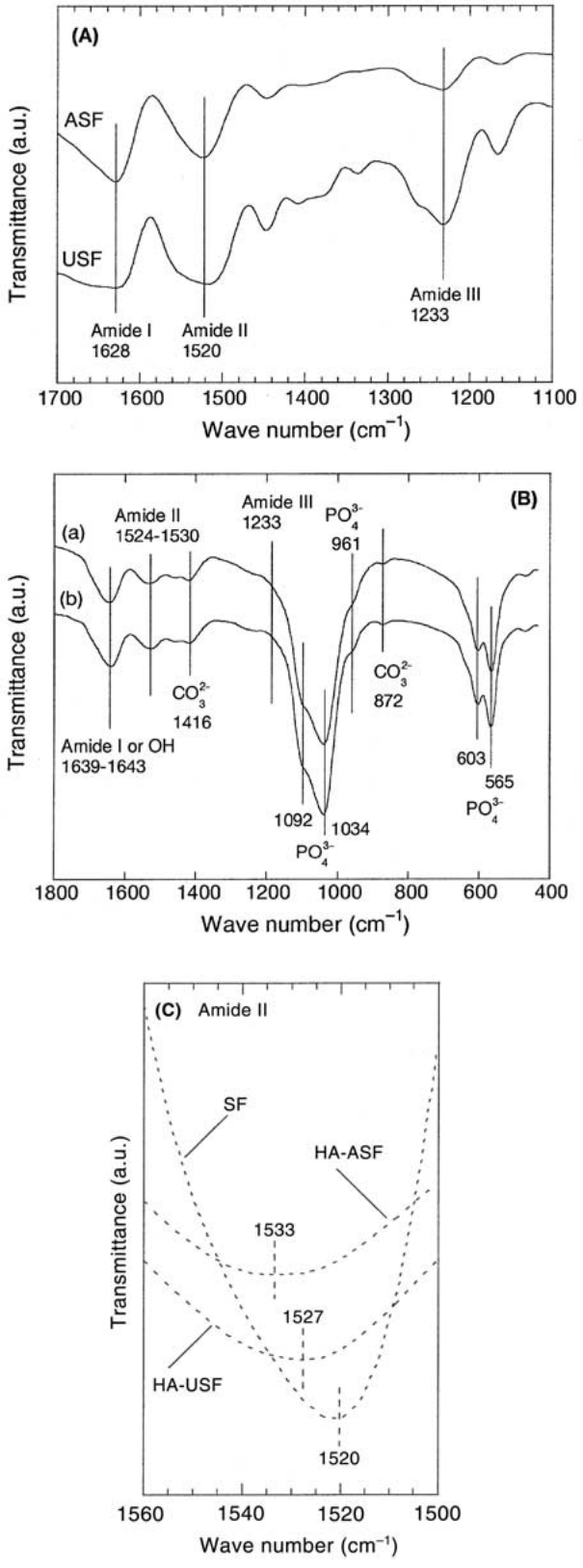

Figure 2 FTIR spectra at different wave number regions: (A) USF and ASF at 1100–1700 cm^{-1}, (B) HA-USF (a) and HA-ASF (b) at 400–1800 cm^{-1}, (C) SF, HA-USF and HA-ASF at 1500–1560 cm^{-1}.

involved in the composite, more intimate cross-linkage between HAp clusters and SF fibrils is built up to form a well developed three-dimensional network extending throughout the composite. HA-ASF seems to show larger pores than HA-USF, as further confirmed by mercury porosimetry.

As shown in Fig. 4, the two samples present similar pore size distribution of a bimodal style, with two maxima at 1.7 and 52 μm for HA-USF and those at 1.7 and 43 μm for HA-ASF, respectively. The results derived from the fractional integration of the distribution curves are listed in Table II. About 70% of the interpores range from 40 to 115 μm in diameter. Bulk density (D_b = sample weight/sample volume) and apparent density ($D_{ap} = 1/(1/D_b - V_{cumu})$, where V_{cumu} is total cumulative pore volume expressed by cm^3/g) are obtained from mercury porosimetry. We calculated total porosity ($P_{total} = 1 - D_b/D_{st}$, $D_{st} = 3.16\,g/cm^3$,

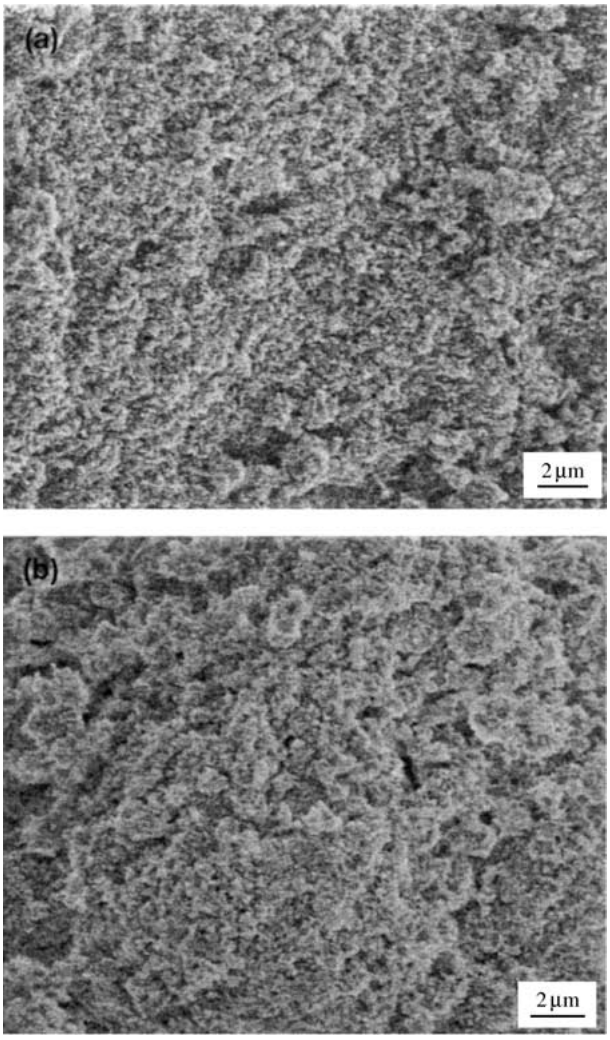

Figure 3 SEM micrographs of (a) HA-USF and (b) HA-ASF composites.

TABLE II Total pore volume pore size distribution

Sample	Total cumulative open pore volume (cm^3/g)	Pore contents at different pore size dimensions (vol %)			
		$< 0.3\,\mu m$	$0.3–10\,\mu m$	$10–40\,\mu m$	$40–115\,\mu m$
HA-USF	0.83	3	11	16	70
HA-ASF	0.91	4	12	14	70

TABLE III Different densities and poroosities

Sample	Bulk density (g/cm^3)	Apparent density (g/cm^3)	Total porosity (%)	Open porosity (%)	Closed porosity (%)	Open/total porosity (%)
HA-USF	0.78	2.26	75	65	10	87
HA-ASF	0.77	2.60	76	70	6	92

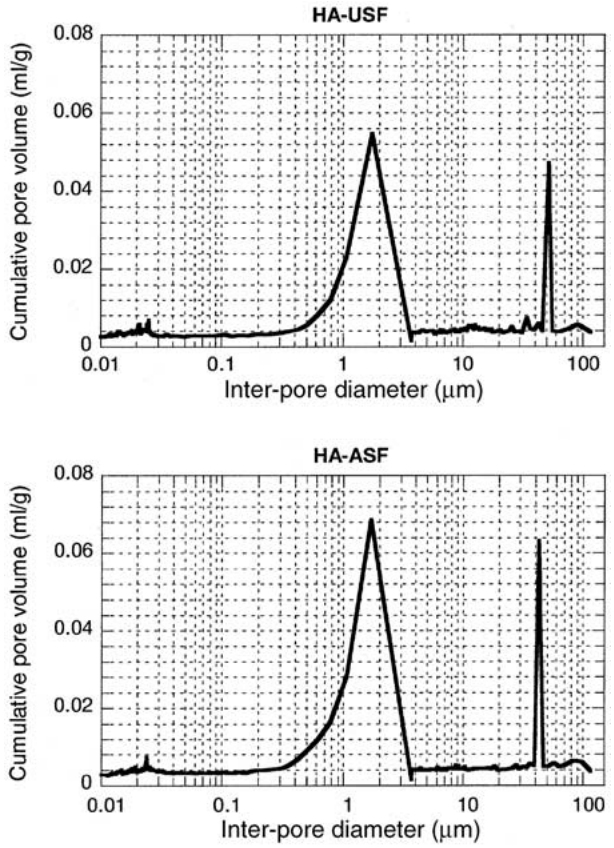

Figure 4 Representative pore size distribution curves of HA-USF and HA-ASF composites.

the density of standard HAp powders), open porosity ($P_{open} = 1 - D_b/D_{ap}$) and closed porosity ($P_{closed} = P_{total} - P_{open}$) [21, 22], as given in Table III. The open porosity amounts to over 87% of the total porosity in both cases. HA-ASF has slightly higher open porosity than HA-USF, attributed to its larger total cumulative open pore volume. Implants with this kind of porous structure analogous with human bone, may facilitate the infiltration of body fluid and blood into the pores to supply nutrient and mineral ions. As a consequence, further bone mineralization and new bone formation can be promoted along with the reinforced adhesion between host tissues and implants [10, 21–24]. Judging from this viewpoint, HA-ASF composite is superior to HA-USF in osteoconduction *in vivo*.

TABLE IV Vickers hardness of the composites. The figures in brackets are standard deviations of the mean

Sample	Vickers hardness number
HA-USF	24.1 (1.7)
HA-ASF	39.2 (4.7)

As shown in Table IV, the Vickers hardness (VHN) of the composites is increased by 63% when ASF used as organic matrix. As for the relationship between microhardness VHN and Young's modulus for HAp-based materials, Bonfield *et al*. revealed empirically that VHN increases with Young's modulus by a square function for natural bone samples and by a closely linear one for HAp-reinforced polyethylene composite [25]. We reasonably assume that the Young's modulus of HA-ASF is higher than that of HA-USF. The mechanical properties of the composite materials are associated with the bonding strength between the component phases. The higher microhardness of HA-ASF than HA-USF, therefore implies that the bonding between HAp and SF is reinforced by the alkali pretreatment. The modified surface of SF by the alkali pretreatment enables SF to provide larger amounts of effective contact points with HAp crystals, so as to intensify the chemical interactions between mineral phase and organic matrix as evidenced by the apparent FTIR blue shift in amide II. Consequently, the more intimate cross-linkage is built up between HAp clusters and SF fibrils, and hence the enhancement in hardness for the composite is achieved.

4. Conclusions

Hydroxyapatite (HAp)-silk fibroin (SF) composites were prepared with either untreated or the alkali pretreated SF (USF or ASF) serving as organic matrix. The alkali pretreatment of SF promotes the preferential growth of HAp crystals along *c*-axis on SF matrix. With ASF involved, the chemical interactions between HAp and SF are intensified, so that the mineral phase can be bound to the organic matrix in a more intimate manner. The highly developed three-dimensional network is built up throughout HAp crystals and SF fibrils, leading to the apparent increase in microhardness of the composite. The composites exhibit porous microstructure with the open porosity of 70% and most of the pores ranging from

40 to 115 μm in diameter, favorable for bony ingrowth *in vivo*.

Acknowledgment

The authors are greatly indebted to Idemitsu Petrochemical Inc. for its donation of silk fibroin and Mr T. Murase for his technical assistance in mercury porosimetry. One of the authors, L. Wang, is also very grateful to Yoshida Scholarship Foundation for its financial support during her doctoral studies in Japan. This work was partially supported by Keio Life Conjugate Chemistry (LCC) Project of Grant-in-Aid for Center of Excellence (COE) research in the 21st Century sponsored by Japanese Ministry of Education, Culture, Sports, Science, and Technology.

References

1. K. S. TENHUISEN, R. I. MARTIN, M. KLIMKIEWICZ and P. W. BROWN, *J. Biomed. Mater. Res.* **29** (1995) 803.
2. M. KIKUCHI, S. ITOH, S. ICHINOSE, K. SHINOMIYA and J. TANAKA, *Biomaterials* **22** (2001) 1705.
3. C. DU, F. Z. CUI, W. ZHANG, Q. L. FENG, X. D. ZHU and K. DE GROOT, *J. Biomed. Mater. Res.* **50** (2000) 518.
4. W. BONFIELD, M. D. GRYNPAS, A. E. TULLY, J. BOWMAN and J. ABRAM, *Biomaterials* **2** (1981) 185.
5. P. T. TON THAT, K. E. TANNER and W. BONFIELD, *J. Biomed. Mater. Res.* **51** (2000) 453.
6. M. WANG and W. BONFIELD, *Biomaterials* **22** (2001) 1311.
7. M. C. CHANG, T. IKOMA, M. KIKUCHI and J. TANAKA, *J. Mater. Sci. Lett.* **20** (2001) 1199.
8. T. FURUZONO, T. TAGUCHI, A. KISHIDA, M. AKASHI and Y. TAMADA, *J. Biomed. Mater. Res.* **50** (2000) 344.
9. L. WANG, R. NEMOTO and M. SENNA, *J. Nanoparticle Res.* **4** (2002) 535.
10. Y. J. YIN, F. ZHAO, X. F. SONG, K. D. YAO, W. W. LU and J. C. LEONG, *J. Appl. Polym. Sci.* **77** (2000) 2929.
11. M. ITO, Y. HIDAKA, M. NAKAJIMA, H. YAGASAKI and A. H. KAFRAWY, *J. Biomed. Mater. Res.* **45** (1999) 204.
12. I. YAMAGUCHI, K. TOKUCHI, H. FUKUZAKI, Y. KOYAMA, K. TAKAKUDA, H. MONMA and J. TANAKA, *J. Biomed. Mater. Res.* **55** (2001) 20.
13. S. H. RHEE and J. TANAKA, *J. Am. Ceram. Soc.* **84** (2001) 459.
14. S. H. RHEE and J. TANAKA, *J. Mater. Sci.: Mater. Med.* **13** (2002) 597.
15. S. J. PARK, K. Y. LEE, W. S. HA and S. Y. PARK, *J. Appl. Polym. Sci.* **74** (1999) 2571.
16. G. FREDDI, P. MONTI, M. NAGURA, Y. GOTOH and M. TSUKADA, *J. Polym. Sci. B: Polym. Phys.* **35** (1997) 841.
17. Q. W. GAO, Z. Z. SHAO, Y. Y. SUN, H. LIN, P. ZHOU and T. Y. YU, *Polym. J.* **32** (2000) 269.
18. K. HAMADA and M. SENNA, *J. Mater. Sci.* **31** (1996) 1725.
19. F. IZUMI and T. IKEDA, *Mater. Sci. Forum* **321** (2000) 198.
20. I. R. GIBSON and W. BONFIELD, *J. Biomed. Mater. Res.* **59** (2002) 697.
21. N. TAMAI, A. MYOUI, T. TOMITA, T. NAKASE, J. TANAKA and T. OCHI, *ibid.* **59** (2002) 110.
22. A. TAMPIERI, G. CELOTTI, S. SPRIO, A. DELCOGLIANO and S. FRANZESE, *Biomaterials* **22** (2001) 1365.
23. K. A. HING, S. M. BEST and W. BONFIELD, *J. Mater. Sci.: Mater. Med.* **10** (1999) 135.
24. P. SEPULVEDA, J. G. P. BINNER, S. O. ROGERO, O. Z. HIGA and J. C. BRESSIANI, *J. Biomed. Mater. Res.* **50** (2000) 27.
25. G. P. EVANS, J. C. BEHIRI, J. D. CURREY, W. BONFIELD, *J. Mater. Sci.: Mater. Med.* **1** (1990) 38.

Received 11 December 2002
and accepted 7 August 2003